Langmuir Article

pubs.acs.org/Langmuir

Hierarchical Porous Materials Made by Drying Complex Suspensions

André R. Studart,*[,†] Julia Studer,[†] Lei Xu,[§] Kisun Yoon,[‡] Ho Cheung Shum,[‡] and David A. Weitz[‡]

[†]*Complex Materials, Department of Materials, ETH Zurich, 8093 Zurich, Switzerland,* [‡]*Department of Physics and School of Engineering and Applied Sciences, Harvard University, Cambridge, Massachusetts, United States, and* [§]*Department of Physics, The Chinese University of Hong Kong, Hong Kong, China*

Received October 4, 2010. Revised Manuscript Received November 26, 2010

Porous structures containing pores at different length scales are often encountered in nature and are important in many applications. While several processing routes have been demonstrated to create such hierarchical porous materials, most methods either require chemical gelation reactions or do not allow for the desired control of pore sizes over multiple length scales. We describe a versatile and simple approach to produce tailor-made hierarchical porous materials that relies solely on the process of drying. Our results show that simple drying of a complex suspension can lead to the self-assembly of droplets, colloidal particles and molecular species into unique 3D hierarchical porous structures. Using a microfluidic device to produce monodisperse templating droplets of tunable size, we prepared materials with up to three levels of hierarchy exhibiting monodisperse pores ranging from 10 nm to 800 μm. While the size of macropores obtained after drying is determined by the size of initial droplets, the interconnectivity between macropores is strongly affected by the type of droplet stabilizer (surfactants or particles). This simple route can be used to prepare porous materials of many chemical compositions and has great potential for creating artificial porous structures that capture some of the exquisite hierarchical features of porous biological materials.

1. Introduction

Porous materials are important in numerous applications, including photovoltaics, catalysis, sensing, filtration, sorption, thermal insulation, fabrication of lightweight structures, and regenerative medicine.[1−7] Pore sizes can vary many orders of magnitude, ranging from 1−20 Å in zeolites[3] to 5−30 nm in mesoporous structures,[8] 1−100 nm in aerogels,[9] and 100 nm to 4 mm in macroporous materials.[10] Combining pore sizes spanning multiple length scales has been explored to fabricate hierarchical porous structures of great technological interest.[11−22] Mesopores (2−50 nm) and macropores (> 50 nm), for example, are desired in catalysis and sensing to simultaneously provide high surface area and enhance the accessibility of gases and liquids to reactive sites. In regenerative medicine, hierarchical structures with large pores (> 300−400 μm) are required for vascularization of the implanted scaffold,[23] while small pores in the range of 50−100 nm are desired to provide physical cues that promote cell migration, proliferation, differentiation, and ultimately fast healing.[24]

Nature has ubiquitous examples of hierarchical structures exhibiting pores spanning from a few nanometers to millimeters in size. This includes, for instance, the intricate aquiferous system of sea sponges,[25] the elaborate network of multiscale canals and

*To whom correspondence should be addressed.

(1) Gratzel, M. Photoelectrochemical cells. *Nature* **2001**, *414*(6861), 338–344.
(2) Gibson, L. J.; Ashby, M. F. *Cellular Solids: Structure and Properties*, 2nd ed.; Cambridge University Press: Cambridge, U.K., 1997; p 510.
(3) Davis, M. E. Ordered porous materials for emerging applications. *Nature* **2002**, *417*(6891), 813–821.
(4) Scheffler, M.; Colombo, P. *Cellular Ceramics: Structure, Manufacturing, Properties and Applications*; Wiley-VCH: Weinheim, Germany, 2005; p 645.
(5) Salgado, A. J.; Coutinho, O. P.; Reis, R. L. Bone tissue engineering: State of the art and future trends. *Macromol. Biosci.* **2004**, *4*(8), 743–765.
(6) Heule, M.; Rezwan, K.; Cavalli, L.; Gauckler, L. J. A miniaturized enzyme reactor based on hierarchically shaped porous ceramic microstruts. *Adv. Mater.* **2003**, *15*(14), 1191−+.
(7) Erlebacher, J.; Seshadri, R. Hard materials with tunable porosity. *MRS Bull.* **2009**, *34*(8), 561–568.
(8) Zhao, D. Y.; Feng, J. L.; Huo, Q. S.; Melosh, N.; Fredrickson, G. H.; Chmelka, B. F.; Stucky, G. D. Triblock copolymer syntheses of mesoporous silica with periodic 50 to 300 angstrom pores. *Science* **1998**, *279*(5350), 548–552.
(9) Fricke, J.; Emmerling, A. Aerogels. *J. Am. Ceram. Soc.* **1992**, *75*(8), 2027–2036.
(10) Studart, A. R.; Gonzenbach, U. T.; Tervoort, E.; Gauckler, L. J. Processing routes to macroporous ceramics: A review. *J. Am. Ceram. Soc.* **2006**, *89*(6), 1771–1789.
(11) Colombo, P.; Vakifahmetoglu, C.; Costacurta, S. Fabrication of ceramic components with hierarchical porosity. *J. Mater. Sci.* **2010**, *45*(20), 5425–5455.
(12) Yang, P. D.; Deng, T.; Zhao, D. Y.; Feng, P. Y.; Pine, D.; Chmelka, B. F.; Whitesides, G. M.; Stucky, G. D. Hierarchically ordered oxides. *Science* **1998**, *282*(5397), 2244–2246.
(13) Rhodes, K. H.; Davis, S. A.; Caruso, F.; Zhang, B. J.; Mann, S. Hierarchical assembly of zeolite nanoparticles into ordered macroporous monoliths using core-shell building blocks. *Chem. Mater.* **2000**, *12*(10), 2832.
(14) Sen, T.; Tiddy, G. J. T.; Casci, J. L.; Anderson, M. W. One-pot synthesis of hierarchically ordered porous-silica materials with three orders of length scale. *Angew. Chem., Int. Ed.* **2003**, *42*(38), 4649–4653.
(15) Kuang, D. B.; Brezesinski, T.; Smarsly, B. Hierarchical porous silica materials with a trimodal pore system using surfactant templates. *J. Am. Chem. Soc.* **2004**, *126*(34), 10534–10535.
(16) Toberer, E. S.; Seshadri, R. Spontaneous formation of macroporous monoliths of mesoporous manganese oxide crystals. *Adv. Mater.* **2005**, *17*(18), 2244–2246.
(17) Vasiliev, P. O.; Shen, Z. J.; Hodgkins, R. P.; Bergstrom, L. Meso/macroporous, mechanically stable silica monoliths of complex shape by controlled fusion of mesoporous spherical particles. *Chem. Mater.* **2006**, *18*(20), 4933–4938.
(18) Sel, O.; Sallard, S.; Brezesinski, T.; Rathousky, J.; Dunphy, D. R.; Collord, A.; Smarsly, B. M. Periodically ordered meso- and macroporous SiO_2 thin films and their induced electrochemical activity as a function of pore hierarchy. *Adv. Funct. Mater.* **2007**, *17*(16), 3241–3250.
(19) Yun, H. S.; Kim, S. E.; Hyeon, Y. T. Design and preparation of bioactive glasses with hierarchical pore networks. *Chem. Commun.* **2007**, No.21, 2139–2141.
(20) Sakatani, Y.; Boissiere, C.; Grosso, D.; Nicole, L.; Soler-Illia, G.; Sanchez, C. Coupling nanobuilding block and breath figures approaches for the designed construction of hierarchically templated porous materials and membranes. *Chem. Mater.* **2008**, *20*(3), 1049–1056.
(21) Kaune, G.; Memesa, M.; Meier, R.; Ruderer, M. A.; Diethert, A.; Roth, S. V.; D'Acunzi, M.; Gutmann, J. S.; Muller-Buschbaum, P. Hierarchically structured titania films prepared by polymer/colloidal templating. *ACS Appl. Mater. Interfaces* **2009**, *1*(12), 2862–2869.
(22) Liu, Q.; Chen, F. L. Self-rising approach to synthesize hierarchically porous metal oxides. *Mater. Res. Bull.* **2009**, *44*(11), 2056–2061.
(23) Karageorgiou, V.; Kaplan, D. Porosity of 3D biomaterial scaffolds and osteogenesis. *Biomaterials* **2005**, *26*(27), 5474–5491.
(24) Vetrone, F.; Variola, F.; de Oliveira, P. T.; Zalzal, S. F.; Yi, J. H.; Sam, J.; Bombonato-Prado, K. F.; Sarkissian, A.; Perepichka, D. F.; Wuest, J. D.; Rosei, F.; Nanci, A. Nanoscale oxidative patterning of metallic surfaces to modulate cell activity and fate. *Nano Lett.* **2009**, *9*(2), 659–665.
(25) Leys, S. P. The choanosome of hexactinellid sponges. *Invertebr. Biol.* **1999**, *118*(3), 221–235.

pores in cortical and trabecular bone,[26] and the multiply bifurcated channels in lungs.[27] Such hierarchical porous structures are designed to exert specific biological and mechanical functions, as well as to optimize flow and exchange reactions. Manmade hierarchical porous materials have yet to achieve the level of sophistication and the tailored architecture of their biological counterparts. Control over the size, shape, and spatial distribution of pores of a few nanometers to millimeters in size potentially enables the fabrication of bioinspired artificial materials with hierarchical porous structures exhibiting novel properties and functions. In this context, simple and general methods to prepare materials with well-controlled pore sizes over multiple length scales are highly desired.

While the small pores in zeolites are defined by the crystalline structure of the aluminosilicate minerals and their synthetic counterparts, the larger pores in meso- and macroporous artificial structures are often incorporated in the material through phase separation phenomena[28] or using templating amphiphilic molecules, particles, droplets, and bubbles to direct the assembly of ions/particles and generate pores upon removal of the template.[8,10,29−33]

Although the formation of pores smaller than a few micrometers using molecules and particles as templates is very well established,[8,12−22,34−36] most three-dimensional (3D) templating methods do not allow for an accurate control over pore sizes larger than 10 μm. Bubbles and droplets are convenient templates to obtain such large pores because they do not require further thermal or chemical processing steps to remove large quantities of templating material. The drawbacks, however, are that conventional emulsification and foaming methods normally lead to broad size distributions[10,37] and that droplets and bubbles are prone to coalescence and Ostwald ripening, which often requires physical or chemical gelation reactions to fix the structure.[30,38,39] Droplet condensation on the surface of polymer solutions is an elegant physical method to produce monodisperse pores of a few micrometers,[40] but is mostly limited to two-dimensional structures and offers little flexibility to tune the pore size.

We report here a very simple and general method to assemble 3D hierarchical porous structures with tailor-made pore sizes by merely drying complex suspensions containing droplets, colloidal particles, and surface active molecules dispersed in a fluid. Given the very different length scales covered by these building blocks, several types of forces are involved in the assembly process, namely, gravitational, colloidal, and molecular forces. While individual control over such forces is usually very challenging, we show that their combined action can be exploited to assemble building blocks of very different sizes into unique 3D structures. Although the formation of polydisperse porous structures from ultrastable particle-stabilized foams and emulsions containing partially gelled networks has been reported in earlier investigations,[31,33,41] we demonstrate that simple drying of less stable surfactant-stabilized systems can lead to surprising and unique porous structures in the absence of any chemical or physical gelation.

2. Materials and Methods

2.1. Materials. Silica particles with diameter of 111 ± 10 nm (grade MP1040, 40 wt % solids aqueous suspension) were acquired from Nissan Chemical Industries Ltd., Tokyo, Japan. Poly(vinyl alcohol) (PVA, 13 000−23 000 g/mol, 87−89% hydrolyzed, Sigma-Aldrich Co., St Louis, MO, USA), toluene (> 99.5% pure, EMD Chemicals, Gibbstown, NJ, USA), octane (Sigma-Aldrich Co.), hexadecane (Sigma-Aldrich Co.), sorbitane monooleate (Span 80, Sigma-Aldrich Co.), glycerol (Sigma-Aldrich Co.), tetraethyl orthosilicate (TEOS, Sigma-Aldrich Co.), trimethylolpropane ethoxylate triacrylate (average number molecular weight ~428 g/mol, Sigma-Aldrich Co.), 1,6-hexanediol diacrylate (Sigma-Aldrich Co.), 2-hydroxy-2-methyl-1-phenyl-1-propanone (Darocur 1173, Ciba Specialty Chemicals Corp., Tarrytown, NY, USA), and nitric acid (1N, Titrisol, Merck) were used as received for the preparation of complex suspensions. Ultrapure water with an electrical resistance higher than 18 MΩ cm was used in all experiments (Milli-Q Synthesis System, Millipore Corp., Billerica, MA, USA).

Monodisperse 400 nm polystyrene particles were synthesized by surfactant-free emulsion polymerization. In a typical synthesis, a mixture of 140 mL of distilled water, 10 mL of styrene (> 99%, inhibited with 4-tert-butylcatechol, Sigma-Aldrich Co.) and 22 mg of potassium persulfate (> 99%, Sigma-Aldrich Co.) is placed in a 200 mL one-neck flask, purged with nitrogen and sonicated for 10 min. Styrene is used without any further purification to remove inhibitors. The reaction flask is tightly sealed with a septum and Teflon tape. The polymerization reaction is carried out by keeping the solution at 70 °C for 20 h under a constant tumbling speed of 60 rpm. The resulting suspension was concentrated to 26 vol % by centrifugation (4400 rpm, Eppendorf 5417R), followed by sonication for 4 min to fully disperse the polystyrene particles (Ultrasonic Processor, GEX 600-5, Ace Glass Inc., Vineland, NJ, USA). Complete dispersion was achieved using 0.010 mol/L of hexadecyltrimethylammonium bromide (CTAB, > 99% pure, Sigma-Aldrich Co.) in the aqueous phase.

2.2. Fabrication of Glass Capillary Microfluidic Devices. Monodisperse oil droplets were generated in glass microcapillary devices using the coflow and flow-focusing geometries shown in

(26) Currey, J. D. The structure of bone tissue. In *Bones: Structure and Mechanics*; Princeton University Press: Princeton, NJ, 2002; pp 3−26.
(27) Reis, A. H.; Miguel, A. F.; Aydin, V. Constructal theory of flow architecture of the lungs. *Med. Phys.* **2004**, *31*(5), 1135–1140.
(28) Nakanishi, K.; Tanaka, N. Sol−gel with phase separation. Hierarchically porous materials optimized for high-performance liquid chromatography separations. *Acc. Chem. Res.* **2007**, *40*(9), 863–873.
(29) Beck, J. S.; Vartuli, J. C.; Roth, W. J.; Leonowicz, M. E.; Kresge, C. T.; Schmitt, K. D.; Chu, C. T. W.; Olson, D. H.; Sheppard, E. W.; McCullen, S. B.; Higgins, J. B.; Schlenker, J. L. A new family of mesoporous molecular-sieves prepared with liquid-crystal templates. *J. Am. Chem. Soc.* **1992**, *114*(27), 10834–10843.
(30) Imhof, A.; Pine, D. J. Ordered macroporous materials by emulsion templating. *Nature* **1997**, *389*(6654), 948–951.
(31) Binks, B. P. Macroporous silica from solid-stabilized emulsion templates. *Adv. Mater.* **2002**, *14*(24), 1824–1827.
(32) Akartuna, I.; Studart, A. R.; Tervoort, E.; Gauckler, L. J. Macroporous ceramics from particle-stabilized emulsions. *Adv. Mater.* **2008**, *20*(24), 4714–+.
(33) Gonzenbach, U. T.; Studart, A. R.; Tervoort, E.; Gauckler, L. J. Ultrastable particle-stabilized foams. *Angew. Chem., Int. Ed.* **2006**, *45*(21), 3526–3530.
(34) Kresge, C. T.; Leonowicz, M. E.; Roth, W. J.; Vartuli, J. C.; Beck, J. S. Ordered mesoporous molecular-sieves synthesized by a liquid-crystal template mechanism. *Nature* **1992**, *359*(6397), 710–712.
(35) Lu, Y. F.; Ganguli, R.; Drewien, C. A.; Anderson, M. T.; Brinker, C. J.; Gong, W. L.; Guo, Y. X.; Soyez, H.; Dunn, B.; Huang, M. H.; Zink, J. I. Continuous formation of supported cubic and hexagonal mesoporous films by sol gel dip-coating. *Nature* **1997**, *389*(6649), 364–368.
(36) Hotta, Y.; Alberius, P. C. A.; Bergstrom, L. Coated polystyrene particles as templates for ordered macroporous silica structures with controlled wall thickness. *J. Mater. Chem.* **2003**, *13*(3), 496–501.
(37) Sen, T.; Tiddy, G. J. T.; Cascic, J. L.; Anderson, M. W. Macro-cellular silica foams: synthesis during the natural creaming process of an oil-in-water emulsion. *Chem. Commun.* **2003**, No.17, 2182–2183.
(38) Choi, S. W.; Cheong, I. W.; Kim, J. H.; Xia, Y. N. Preparation of uniform microspheres using a simple fluidic device and their crystallization into close-packed lattices. *Small* **2009**, *5*(4), 454–459.
(39) Choi, S. W.; Xie, J. W.; Xia, Y. N. Chitosan-based inverse opals: Three-dimensional scaffolds with uniform pore structures for cell culture. *Adv. Mater.* **2009**, *21*(29), 2997.
(40) Boker, A.; Lin, Y.; Chiapperini, K.; Horowitz, R.; Thompson, M.; Carreon, V.; Xu, T.; Abetz, C.; Skaff, H.; Dinsmore, A. D.; Emrick, T.; Russell, T. P. Hierarchical nanoparticle assemblies formed by decorating breath figures. *Nat. Mater.* **2004**, *3*(5), 302–306.
(41) Gonzenbach, U. T.; Studart, A. R.; Tervoort, E.; Gauckler, L. J. Macroporous ceramics from particle-stabilized wet foams. *J. Am. Ceram. Soc.* **2007**, *90*(1), 16–22.

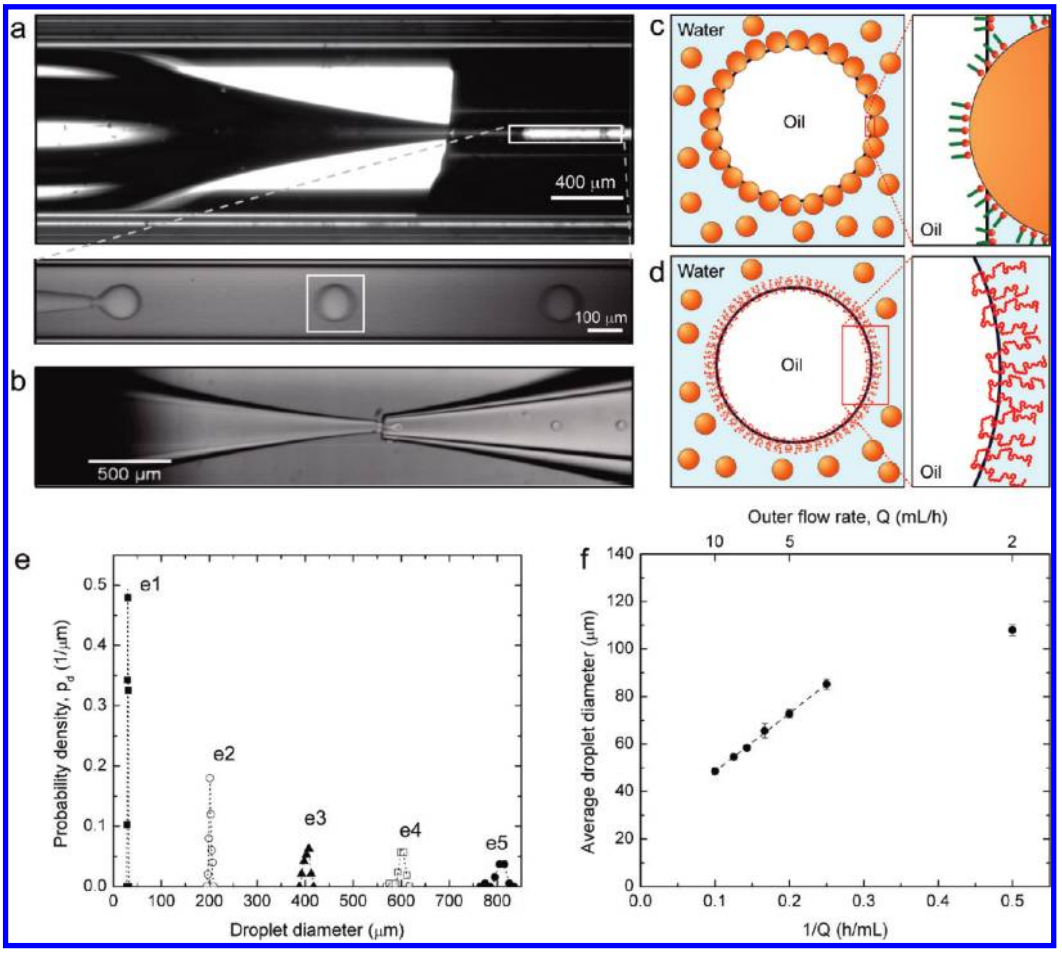

Figure 1. Formation of complex suspensions containing droplets, colloidal particles, and surface active molecules in glass microfluidic devices. (a,b) Droplet formation in microfluidic devices in coflow and flow-focusing configurations, respectively. In the coflow geometry, the tip of the inlet capillary is inserted in a collecting capillary of fixed diameter. In the flow-focusing geometry, the tip of the inlet capillary is positioned a few tens of micrometers away from a tapered collecting capillary of small diameter, enabling the formation of smaller droplet sizes. (c,d) The resulting droplets can be stabilized by adsorbing either (c) *in situ* hydrophobized colloidal particles or (d) surface active molecules at the oil−water interface. (e) Droplet size distributions obtained with different device geometries and flow conditions (see Materials and Methods for details). (f) Average droplet diameter as a function of the flow rate Q and $1/Q$ for one particular flow-focusing device (inlet tip diameter: 57 μm, collecting tip diameter: 116 μm, inner flow rate: 50 μL/h).

Figure 1a,b. In these geometries, a tapered cylindrical inlet capillary is fitted into an outer square capillary to enable the simultaneous flow of two immiscible fluids through the device. A square capillary with inner diameter of 1.1 mm and a cylindrical inlet capillary with outer diameter of 1.0 mm were used to enable easy assembly, while maintaining a good alignment of the capillaries. Tapered cylindrical capillaries were produced by axial heating (World Precision Instruments, Sarasota, FL, USA) in a micropipet puller (Model P-97 Flaming/Brown puller, Sutter Instruments, Novato, CA, USA).[42] Capillaries with initial inner diameters of either 580 or 200 μm were used. The heating conditions were adjusted to produce inlet capillaries with inner diameters varying from 10 to 210 μm at the tip. In the coflow geometry, the tip of the tapered inlet capillary was inserted into a collecting capillary with an inner diameter of 200 μm (Figure 1a), whereas in the flow-focusing devices the inlet capillary tip was positioned a few tens of micrometers away from a tapered collecting capillary (Figure 1b). The tapered collecting capillaries used in the flow-focusing devices were prepared using round (200 or 580 μm inner diameter) or squared (1 mm inner side) capillaries following the same procedure described for the inlet capillaries. The inner diameter of the tapered capillary tip was varied between 24 and 834 μm.

2.3. Emulsification in Microcapillary Devices. Droplets were produced in the dripping mode[43] by pumping the oil phase through the cylindrical inlet capillary and an aqueous suspension of colloidal particles through the outer square capillary, as indicated in Figure 1. The inner and outer flow rates used for droplet formation were adjusted in the ranges of 100−500 and 500−36000 μL/min, respectively, using syringe pumps (Harvard apparatus, PHD 2000 Programmable, Holliston, MA, USA). To illustrate the broad range of monodisperse droplets that can be created, we used a mixture of 99 wt % 1,6-hexanediol diacrylate and 1 wt % 2-hydroxy-2-methyl-1-phenyl-1-propanone as the oil phase. Table 1 shows the device geometry and the flow conditions applied to obtain the droplet sizes depicted in Figure 1e. The droplet sizes were evaluated from optical images using the software Image J (version 1.42q, National Institutes of Health, USA).

Either silica or polystyrene was used as colloidal particles in the aqueous continuous phase. The concentrations of particles, surface active molecules and inorganic molecular species indicated

(42) Utada, A. S.; Lorenceau, E.; Link, D. R.; Kaplan, P. D.; Stone, H. A.; Weitz, D. A. Monodisperse double emulsions generated from a microcapillary device. *Science* **2005**, *308*(5721), 537–541.

(43) Utada, A. S.; Fernandez-Nieves, A.; Stone, H. A.; Weitz, D. A. Dripping to jetting transitions in coflowing liquid streams. *Phys. Rev. Lett.* **2007**, *99*(9), 094502.

Table 1. Device Geometries and Flow Conditions Used to Obtain the Droplet Size Distributions Shown in Figure 1e[a]

	e1	e2	e3	e4	e5
average droplet size (μm)	30.0	201.7	403.3	599.1	806.6
standard deviation, σ (μm)	0.7	2.2	5.6	7.9	10.3
polydispersity (%)	2.3	1.1	1.4	1.3	1.3
collecting tip diameter (μm)	24.4	300	450	834	834
inlet tip diameter (μm)	20.6	49.2	63.7	43.2	43.2
outer flow rate (μL/h)	500	10000	500	36000	12000
inner flow rate (μL/h)	100	500	100	500	500

[a] The average droplet sizes and standard deviations were obtained by fitting the data to Gaussian distributions.

here were all calculated with respect to the water used as the outer fluid.

A high-speed camera (Vision Research, Wayne, NJ, USA) coupled to an optical microscope (model DM IRB, Leica Microsystems, Wetzlar, Germany) was used to observe droplet formation in the microcapillary device.

2.4. Emulsion Stabilization. To obtain particle-stabilized droplets, silica particles were *in situ* hydrophobized to adsorb on the surface of freshly created oil droplets along the collecting capillary. Partially hydrophobic particles were generated by adsorbing CTAB on the silica surface at pH 8.[33,44] A concentration of 0.0004 mol/L CTAB in the aqueous phase was sufficient to hydrophobize the surface without leading to extensive particle coagulation in the suspension. The concentration of silica particles in the aqueous phase was varied between 15 and 22 vol %. In a typical experiment, droplets were formed using flow rates of 400 and 4000 μL/h for the inner and outer fluids, respectively. Toluene was used as the oil phase in most of the experiments with particle-stabilized droplets. To confirm the adsorption of modified silica particles on the droplet surface, we also used a photosensitive oil mixture consisting of 45 wt % 1,6-hexanediol diacrylate (monomer), 22.5 wt % trimethylolpropane ethoxylate triacrylate (monomer), 7.5 wt % 2-hydroxy-2-methyl-1-phenyl-1-propanone (initiator), and 25 wt % toluene (diluent) as the oil phase during droplet formation. After collection onto a glass substrate, the oil droplets were exposed to a 325 nm ultraviolet lamp for about 3 min to polymerize the photosensitive oil mixture.

Surfactant-stabilized droplets were produced using either PVA or CTAB as surface active molecules. Complex suspensions containing PVA-stabilized droplets were prepared using octane as the oil phase and a suspension of 1−2 wt % PVA and 15 vol % silica particles as the continuous aqueous phase. Conversely, complex suspensions containing CTAB-stabilized droplets were prepared using octane as the oil phase and a mixture of polystyrene particles (10.5 vol %), CTAB (0.045 mol/L) and TEOS (0.29−1.00 mol/L) as the continuous aqueous phase. In order to ensure complete hydrolysis of TEOS into silicate species, the aqueous fluid was prepared in multiple steps. In a typical experiment, 1.42 g of distilled water, 10 mg of HNO_3 1 M aqueous solution, and 0.45 g of TEOS were mixed (in this sequence) and stirred for approximately 30 min. The low pH of this initial suspension (<3) led to complete hydrolysis of TEOS and prevented undesired condensation reactions between the silicate species formed. The resulting aqueous solution was then mixed with 1.8 g of a 26 wt % polystyrene aqueous suspension to form suspension "A". In another vial, 0.11 g of CTAB was dissolved in 3.35 g of distilled water with the help of an ultrasonic probe. The resulting CTAB solution was then mixed with 1.85 g of the 26 wt % polystyrene aqueous suspension and with 10 mg of HNO_3 1 M aqueous solution (in this sequence) to form suspension "B". By mixing suspensions "A" and "B" we finally obtained an aqueous suspension containing 10.5 vol % polystyrene particles dispersed in an aqueous solution of 0.045 mol/L CTAB and 0.29 mol/L silicate species. Aqueous suspensions with higher concentrations of TEOS were prepared using a similar procedure. During droplet formation, flow rates of 400 and 4000 μL/h were typically used for the inner and outer fluids, respectively.

2.5. 3D Substrates. The glass substrates used to create 3D porous structures (Figure 5) were made of a photostructurable glass ceramic (Foturan) and were kindly supplied by Mikroglas Chemtech GmbH (Mainz, Germany).

2.6. Microscopic Analysis. An optical microscope (model DM RX, Leica Microsystems, Wetzlar, Germany) was used to characterize both wet and dried structures and to assess the dynamics of the drying process. Some of the dried structures were also characterized in a field emission scanning electron microscope (FESEM, Supra 55VP, Carl Zeiss NTS GmbH, Oberkochen, Germany) after coating the samples with a thin layer of platinum.

3. Results and Discussion

The well-controlled flow conditions achieved in microfluidic devices enables the preparation of monodisperse droplets at a speed of approximately 120−180 droplets/s. Monodisperse droplets with sizes ranging from 30 to 850 μm were easily prepared by varying mainly the diameter of the collecting capillary tip and the applied flow rates, Q (Figure 1e,f). Droplets were formed under dripping mode in all the experiments. The droplet diameter depends linearly on $1/Q$ for most of the flow rates applied in a particular flow-focusing device, as shown in Figure 1f. Deviation from this linear trend only occurred when the droplets size approached the diameter of the collecting capillary tip, indicating that in this case the size is determined by the device geometry rather than the flow conditions applied. The dependence of droplet size on $1/Q$ is in qualitative agreement with the behavior expected from balancing shearing and interfacial forces acting on the droplet surface close to the capillary tip.[45]

The complex suspensions obtained from the microfluidic devices were stable and could be transferred from the collecting capillary directly onto glass substrates. The selection of surface active molecules that can efficiently stabilize droplets without interfering with the dispersion of the colloidal particles is crucial to avoid droplet coalescence while transferring the suspensions to the substrate. When added in appropriate amounts (see Materials and Methods), PVA or CTAB fulfilled these criteria. A few seconds after deposition of the suspension on the substrate, droplets creamed to the air−water interface due to the lower specific gravity of the oil phase in comparison to that of water. This buoyant effect led to the formation of curved air−water interfaces between droplets, which ultimately induced their self-assembly into ordered hexagonal arrays (Figure 2a,b and video S1 in the Supporting Information). In addition to the monolayer structures shown in Figure 2, multilayers could also be formed by geometrically confining the droplets within the wells of a structured substrate or on a concave glass.[38] The thickness of the multilayer structure could be controlled by changing the droplet concentration under such confined conditions.

(44) Studart, A. R.; Shum, H. C.; Weitz, D. A. Arrested coalescence of particle-coated droplets into nonspherical supracolloidal structures. *J. Phys. Chem. B* **2009**, *113*(12), 3914–3919.

(45) Umbanhowar, P. B.; Prasad, V.; Weitz, D. A. Monodisperse emulsion generation via drop break off in a coflowing stream. *Langmuir* **2000**, *16*(2), 347–351.

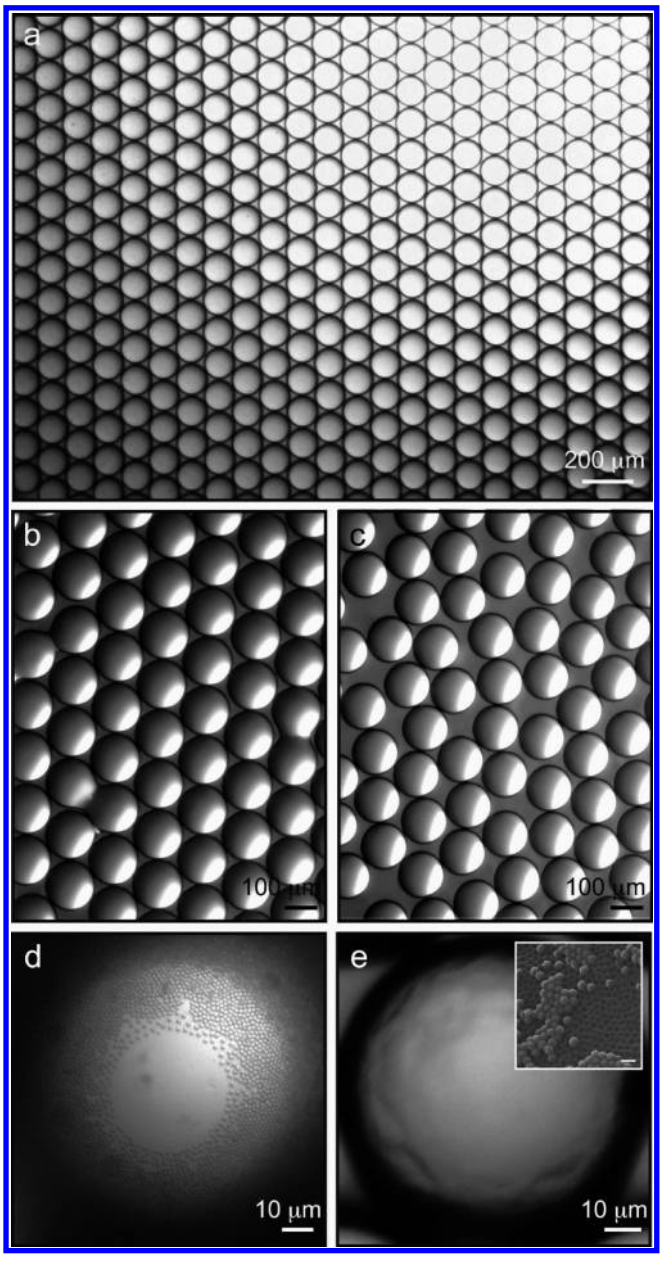

Figure 2. Self-assembly of droplets and colloidal particles after deposition of complex suspensions onto glass substrates. (a) Assembly of PVA-stabilized octane droplets into ordered 2D arrays from suspensions containing 15 vol % SiO_2 colloidal particles dispersed in the aqueous continuous phase. (b,c) Assembly of SiO_2-stabilized toluene droplets into (b) ordered and (c) disordered structures from suspensions containing 22 vol % SiO_2 and 0.0004 mol/L CTAB. (d) Top view of a CTAB-stabilized oil droplet that creamed to the air−water interface. Two micrometer polystyrene particles (10 vol %) were intentionally added to this suspension to show the depletion of particles from the droplet top surface. (e) The buckled surface of a particle-coated toluene droplet formed in suspensions containing 15 vol % SiO_2 particles and 0.0004 mol/L CTAB. The inset in panel e shows a scanning electron microscopy image of partially hydrophobized silica particles adsorbed on the surface of a polymerized oil droplet (see experimental details in Materials and Methods). The large imprints formed on the droplet surface indicate that particles were positioned deeply into the oil−water interface. Scale bar: 200 nm in inset e.

Droplets stabilized with PVA or CTAB promptly self-assembled into compact structures upon deposition of the complex suspension on glass substrates. In contrast, particle-stabilized droplets were less mobile at the air−water interface, most likely due to weakly attractive interactions between the partially hydrophobic particles. As a result of this lower mobility, droplets stabilized with particles were able to form both ordered and disordered arrays (Figure 2b,c). For droplets to be fully stabilized by particles, particle concentrations need to be above 20 vol %. At lower concentrations, droplets tended to partially coalesce into nonspherical structures.[44] This suggests that the formation of an attractive network of particles throughout the continuous phase is required to keep droplets apart and prevent their coalescence, which is in agreement with observations made in other particle-stabilized systems containing surface active molecules.[33,46,47] The fact that emulsification in microfluidic devices occurs in much shorter time scales if compared to mechanical frothing processes might be another reason for the need of such high particle concentrations. High particle concentrations should favor fast adsorption of modified particles to the oil−water interface, preventing coalescence in short time scales.

The approach used for droplet stabilization has a direct effect on the distribution of colloidal particles in the complex suspensions. Particle-free regions are observed on the top of buoyant droplets stabilized by surface active molecules (Figure 2d). Particles are depleted from the uppermost part of the creaming droplet due to repulsive interactions with the surfactant-stabilized oil−water interface. As a result, only a thin aqueous layer separates the oil droplet from the air−water interface in this system. In contrast, droplets stabilized by the *in situ* hydrophobized particles exhibited a textured coating of particles on the surface. The buckling observed at the droplet surface is in agreement with the presence of particles adsorbed at the oil−water interface (Figure 2e). The adsorption of modified particles at the interface was confirmed by scanning electron microscopy of polymerized droplets (Figure 2e, inset). It is important to note that in both systems, the vast majority of colloidal particles remain distributed throughout the continuous aqueous phase.

Drying of these complex suspensions leads to unique hierarchical porous structures. Remarkably, the initial wet structure of droplets and colloidal particles deposited on substrates can be totally preserved upon evaporation of the water and oil immiscible phases for both surfactant-stabilized and particle-stabilized systems.

Three major stages are identified in the drying process. The first and most important stage for preserving the initial structure is the evaporation of the excess liquid from the continuous phase and the formation of a close packing of particles between droplets. This process starts from the edges and propagates in the form of a first drying front toward the center of the deposited complex suspension. The evaporation of excess water from the continuous phase causes extensive jamming of the colloidal particles into compact structures around the oil droplets, as schematically illustrated in Figure 3a for the case of particle-stabilized droplets. At this point, a minimum initial concentration of particles of approximately 10−15 vol % is required to ensure jamming throughout the continuous phase and thus avoid droplet coalescence during drying. Particle jamming was indicated by the loss of mobility of the initially Brownian colloidal particles as the first drying front propagated through the structure (region b2 in Figure 3b and videos S2 and S3 in the Supporting Information). In the particle-stabilized system, the partially hydrophobic particles

(46) Akartuna, I.; Studart, A. R.; Tervoort, E.; Gonzenbach, U. T.; Gauckler, L. J. Stabilization of oil-in-water emulsions by colloidal particles modified with short amphiphiles. *Langmuir* **2008**, *24*(14), 7161–7168.
(47) Gonzenbach, U. T.; Studart, A. R.; Tervoort, E.; Gauckler, L. J. Stabilization of foams with inorganic colloidal particles. *Langmuir* **2006**, *22*(26), 10983–10988.

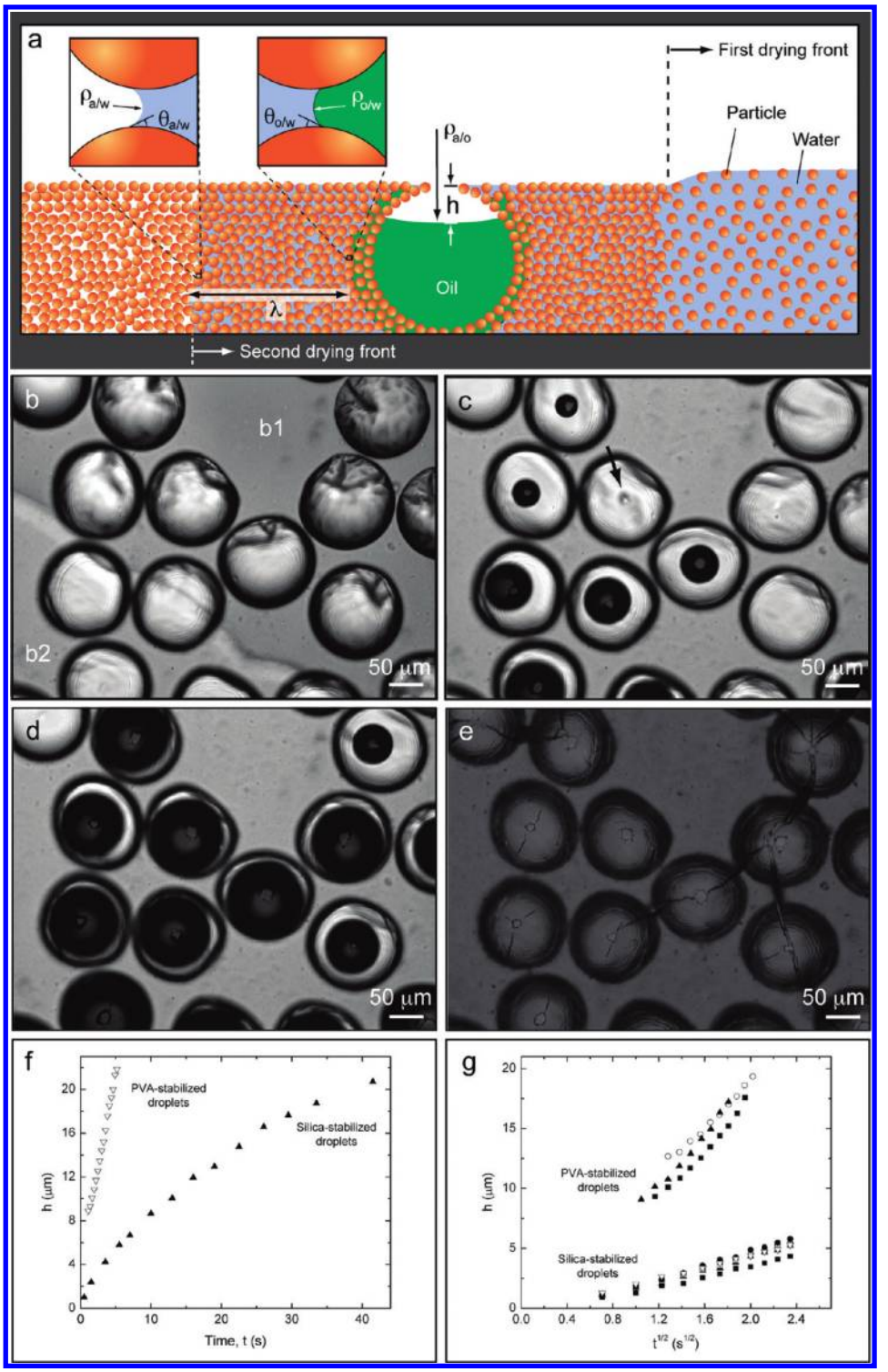

Figure 3. Dynamics of the drying process of complex suspensions. (a) Scheme illustrating the evacuation of the droplet inner fluid into the surrounding particle pack (see text). (b−d) Optical microscopy images taken (b) 22, (c) 58, and (d) 114 s after deposition of a suspension containing particle-stabilized toluene droplets on a glass substrate (0.0004 mol/L CTAB, 22 vol % 110 nm silica particles). Image b shows the first drying front moving across the suspension from the bottom left to the top right of the image. Regions where colloidal particles within the continuous phase exhibited Brownian motion or formed a jammed particle network are indicated by b1 and b2, respectively. The arrow in c indicates the moment when the thin aqueous film between the droplet top surface and the uppermost air−water interface is ruptured. The structure after complete drying is shown in e. Graphs f and g display the increase of the depth h (indicated in a) as a function of time, t, and $t^{1/2}$, respectively, for complex suspensions containing surfactant (PVA)-stabilized droplets and particle (silica)-stabilized droplets. Different symbols in g correspond to different droplets in the drying suspension.

exhibited strong Brownian motion before propagation of the first drying front, indicating that their weakly attractive nature is not sufficient to form a particle network throughout the continuous phase. A wet arrested structure of packed oil droplets and colloidal particles embedded in a continuous aqueous phase is obtained after this first drying stage (Figure 3a). Such jamming and

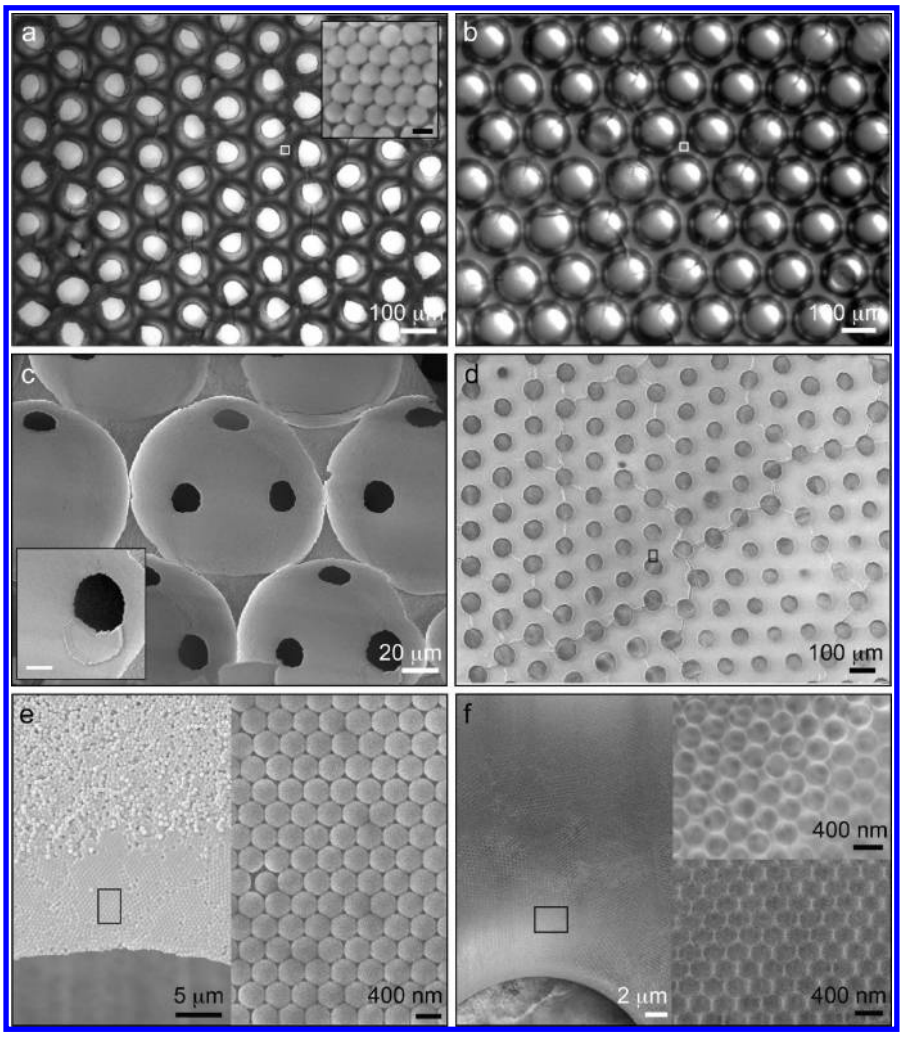

Figure 4. Three dimensional hierarchical porous structures formed by drying complex suspensions. (a,b) Optical images of (a) open and (b) closed ordered arrays obtained after drying complex suspensions containing (a) 125 μm octane droplets and 110 nm silica particles (15 vol %) dispersed in a 1 wt % PVA aqueous solution and (b) 140 μm silica-coated toluene droplets and 110 nm silica particles (22 vol %) dispersed in a 0.0004 mol/L CTAB aqueous solution. The inset in panel a shows an FESEM image of the silica particles located between the open and closed macropores after complete drying. (c) Internal windows between macropores for the structure shown in panel a. The inset indicates a remainder of the pore wall, which ruptures during the droplet evacuation process to generate a pore window. (d) FESEM image of open porous structure formed after drying complex suspensions containing 150 μm octane droplets and 400 nm polystyrene particles (10.5 vol %) dispersed in an aqueous solution containing 0.045 mol/L CTAB and 0.29 mol/L silicate species. FESEM images (e) and (f) display representative magnified views of the region close to a macropore in (d). In the as-dried material (e), ordered and disordered arrays of 400 nm polystyrene particles are formed close and further away from the macropore opening, respectively. Thermal decomposition of the polystyrene particles leads to the formation of regular and disordered arrays of 400 nm pores between the 140 μm pores (f). The thickness of the resulting silica walls can be tuned by changing the concentration of TEOS in the initial aqueous solutions (top right in f: 1 mol/L TEOS; bottom right in f: 0.29 mol/L TEOS). Scale bars: 100 nm in inset (a) and 10 μm in inset (c).

structural arresting effects were also evident in the surfactant-stabilized system (video S3 in the Supporting Information).

Drying proceeds in the second stage with air invading the network of jammed particles surrounding the oil droplets, causing the continuous aqueous phase to recede and form curved air−water interfaces within the particle pack.[48] This is schematically illustrated in Figure 3a in the form of a second drying front. The curved air−water interface of the receding aqueous phase and the curved oil−water interface of the droplets give rise to a pressure difference ΔP across the particle pack that can be described as follows:

$$\Delta P = \frac{\gamma_{a/w}}{|\rho_{a/w}|} - \frac{\gamma_{o/w}}{|\rho_{o/w}|} \quad (1)$$

where $\gamma_{a/w}$ and $\gamma_{o/w}$ are the air−water and oil−water interfacial tensions, respectively, and $\rho_{a/w}$ and $\rho_{o/w}$ are the radii of curvature of the air−water and oil−water interfaces, respectively (Figure 3a).

The pressure difference ΔP operates radially throughout the droplet surface and tends to suck the oil phase from the droplets into the continuous phase. Initially, this pressure difference does not cause any fluid flow due to the droplet's symmetry. As the aqueous phase continues to recede, the thin aqueous film that separates the top surface of the oil droplet from the uppermost air−water interface is ruptured, unbalancing the pressure difference across the droplet surface and ultimately leading to the evacuation of the oil phase from the droplets into the interstices of the surrounding particle pack (Figure 3a). This phenomenon is thoroughly described in a

(48) Xu, L.; Davies, S.; Schofield, A. B.; Weitz, D. A. Dynamics of drying in 3D porous media. *Phys. Rev. Lett.* **2008**, *101*(9), 094502.

recent study on drying of model complex suspensions in a confocal microscope.[49]

The evacuation process is exemplified in Figure 3b−e for complex suspensions containing particle-stabilized droplets (see also video S2 in the Supporting Information). As soon as the thin aqueous film between the droplet and the uppermost surface of the suspension is ruptured, the evacuation process is initiated, as indicated with an arrow for one of the droplets in Figure 3c. The same behavior is also observed for complex suspensions containing surfactant-stabilized droplets (see video S3 in the Supporting Information). Interestingly, the evacuation process is remarkably faster in the surfactant-stabilized system than in the particle-stabilized emulsions, as indicated by the kinetic data shown in Figure 3f. Despite the difference in evacuation speed, in both systems the depth h of the oil phase with respect to the droplet top surface (Figure 3a) exhibits a linear dependence with the square root of the elapsed time, $t^{1/2}$ (Figure 3g).

To gain further insight into the drying process and its effect on the structure of the final porous material, we analyzed the dynamics of the evacuation process for the surfactant- and particle-stabilized emulsions. The pressure-driven flow of the droplet fluid into the interstices of the surrounding particle pack can be described by Darcy's law:[49]

$$q = \frac{Ak}{\eta}\nabla P \tag{2}$$

where q is the volumetric flow rate, k is the permeability of the particle pack, η is the fluid viscosity, ∇P is the pressure gradient across the particle pack, and A is the cross-sectional area perpendicular to the flow.

Using Darcy's law, we estimate that, at the beginning of the evacuation process ($h \ll R$), the depth h of the oil phase should vary with time according to the following equation (see Supporting Information):

$$h(t) = \left(\frac{4Rk\nabla P}{\eta}\right)^{1/2} t^{1/2} \tag{3}$$

The fact that the depth h predicted from this equation exhibits the same time dependence as that obtained experimentally (Figure 3f,g) confirms that the evacuation process is indeed driven by the convective flow of the droplet fluid into the surrounding particle pack.

A comparison between the experimentally determined slopes of the h versus $t^{1/2}$ data and the slope $(4Rk\nabla P/\eta)^{1/2}$ obtained from eq 3 provides further information about the particle pack around the droplets and the capillary pressure driving the evacuation process.

To estimate the permeability k in eq 3, we use the Kozeny−Carman equation, $K \cong {r_p}^2(1-\phi)^3/(45\phi^2)$, where r_p is the particle radius, and ϕ is the volume fraction of particles. Introducing the permeability k into eq 3 and assuming a pressure gradient $\nabla P = \Delta P/\lambda = (\gamma_{a/w}\cos\theta_{a/w} - \gamma_{o/w}\cos\theta_{o/w})/(0.3r_p\lambda)$ (see Figure 3a and Supporting Information), we predict a slope, s, for the h versus $t^{1/2}$ data as follows:

$$s = [(0.296Rr_p(1-\phi)^3(\gamma_{a/w}\cos\theta_{a/w} - \gamma_{o/w}\cos\theta_{o/w}))/(\eta\lambda\phi^2)]^{1/2} \tag{4}$$

where $\theta_{a/w}$ and $\theta_{o/w}$ are the contact angles formed by the solid particles at the air−water and oil−water interfaces, respectively (Figure 3a).

To compare eq 4 with the experimentally determined slopes of the curves shown in Figure 3g, the parameters R, r_p, η, and λ were directly assessed in our experiments (see Supporting Information), while the interfacial tensions $\gamma_{a/w}$ and $\gamma_{o/w}$ were estimated on the basis of literature data.

For the PVA-stabilized system, the hydrophilic silica particles dispersed in the continuous phase are expected to be fully wetted by water. Thus, it is reasonable to assume that the contact angles $\theta_{a/w}$ and $\theta_{o/w}$ equal zero in this case. On the basis of literature data,[50,51] values of 30 and 7 mN/m for the air−water ($\gamma_{a/w}$) and oil−water interfacial tensions ($\gamma_{o/w}$), respectively, are good approximations for the PVA concentration and degree of hydrolysis used in our study (2 wt % and 88%, respectively). Equation 4 was then used to estimate the volume fraction of particles in the pack around droplets, ϕ. For slopes in the range of 9.6−10.8 obtained experimentally, we achieve ϕ values varying from 0.742 to 0.758. These values are close to the volume fraction of equally sized spheres in a dense hexagonal packing (0.74). The observation that the silica particles indeed form ordered hexagonal structures around the droplets (Figure 4a) indicates that our model correctly captures the dynamics of the evacuation process.

Considering the good agreement between theory and experiments obtained for the PVA-stabilized system, we extended the model to the particle-stabilized emulsions. In this case, a volume fraction ϕ of 0.74 is taken based on the hexagonal dense packing of particles observed experimentally (Figure 4a). By approximating the interfacial tension $\gamma_{a/w}$ and $\gamma_{o/w}$ using literature data,[33,46] the only undetermined variables remaining are the contact angles $\theta_{a/w}$ and $\theta_{o/w}$. Assuming that $\theta_{a/w} \sim \theta_{o/w}$,[52] a comparison between the experimental and theoretical slopes s leads to a contact angle within the range 86−88°. The deep dimples left by the interfacially adsorbed silica particles on the surface of droplets after polymerization of the oil phase (Figure 2e) suggests that the estimated range for the contact angle is very plausible.

Given the fact that all the other variables in eq 4 exhibit similar values for both surfactant- and particle-stabilized suspensions, the 4-fold slower evacuation observed for the particle-stabilized system is primarily caused by the high contact angle of the hydrophobized silica particles at the air−water and oil−water interfaces. The different contact angles of the silica particles in both systems leads to a markedly different pressure difference ΔP across the particle pack around droplets. Using eq 1, we estimate a pressure drop in the range 60−100 kPa in the particle-stabilized system, as opposed to a pressure drop of approximately 1500 kPa for the surfactant-stabilized system. The magnitude of pressure drop in the particle pack is expected to directly affect the formation of interconnecting windows between the macropores during drying. The depletion of particles observed at the top of droplets stabilized with PVA (Figure 2d) is also likely to occur between laterally touching droplets, thus leading to open windows after drying. Opening of windows between macropores is favored by the very high pressure drop estimated for this system. The formation of connections between adjacent droplets during the evacuation

(49) Xu, L.; Berges, A.; Lu, P. J.; Studart, A. R.; Schofield, A. B.; Oki, H.; Davies, S.; Weitz, D. A. Drying of complex suspensions. *Phys. Rev. Lett.* **2010**, *104* (12), 128303.

(50) Defeijter, J. A.; Benjamins, J. Adsorption behavior of PVA at the air−water-interface. 0.1. Applicability of the Gibbs adsorption equation. *J. Colloid Interface Sci.* **1981**, *81*(1), 91–107.

(51) Lankveld, J. M.; Lyklema, J. Adsorption of polyvinyl alcohol on paraffin-water interface.1. Interfacial tension as a function of time and concentration. *J. Colloid Interface Sci.* **1972**, *41*(3), 454–465.

(52) Arnaudov, L. N.; Cayre, O. J.; Stuart, M. A. C.; Stoyanov, S. D.; Paunov, V. N. Measuring the three-phase contact angle of nanoparticles at fluid interfaces. *Phys. Chem. Chem. Phys.* **2010**, *12*(2), 328–331.

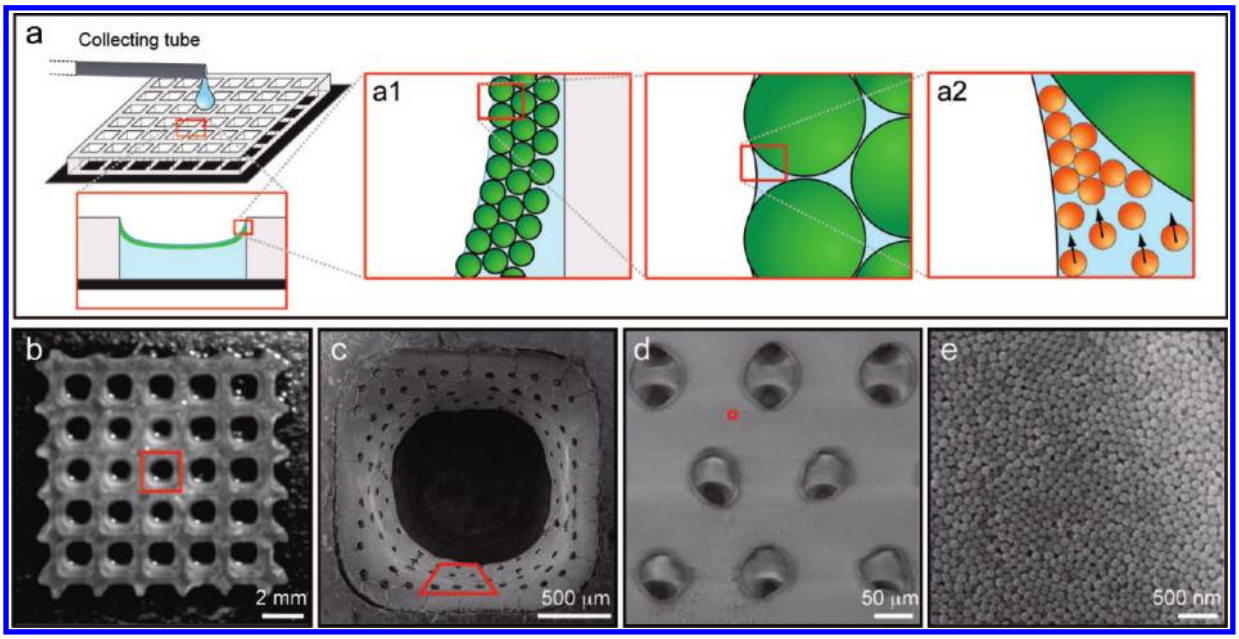

Figure 5. (a) Scheme illustrating the drying-induced multiscale assembly process in which (a1) creaming oil droplets are deposited on the walls of periodic holes of a glass substrate and (a2) colloidal particles are driven by capillary flow into the interstices of deposited droplets as drying proceeds. (b−e) FESEM images of hierarchical porous structure resulting from the multiscale assembly of complex suspensions containing 120 μm octane droplets and 110 nm silica particles (15 vol %) dispersed in 1 wt % PVA. In the sequence from left to right, the red rectangles indicate the areas magnified in the next adjacent image.

process is confirmed by the correlated oscillations of the liquid interface on the top of neighboring droplets (see video S4 in the Supporting Information). We also observed that the high pressure drop across the continuous phase of the PVA-stabilized suspension can in some cases lead to the rupture of the layer of particles possibly present between adjacent droplets, as shown in the inset of Figure 4c. In contrast, only a few interconnecting windows are formed between macropores in the particle-stabilized system.

In the final stage of drying, the oil and aqueous fluids located within the interstices of the particle pack are evaporated to form random or ordered hierarchical porous structure that perfectly mimics the colloidal architecture of the precursor suspensions (Figure 4a−c). In addition to a close match between the size of the initial droplets and the size of resulting macropores (Figure S1 in the Supporting Information), the porous structures obtained also reflect the initial distribution of colloidal particles and droplets of the original complex suspension. The particle-free regions formed between and on the top surface of surfactant-stabilized droplets (Figure 2d) lead to open windows in the dry porous structure, whereas the particle-coated droplets from the particle-stabilized systems (Figure 2e) result in fully closed macropores after drying (Figure 4a,b, respectively). The closely packed colloidal particles between these macropores give rise to nanosized interstices, establishing a second hierarchy of pores in the structure (inset of Figure 4a). As the colloidal particles in the as-dried structures are held together by relatively weak van der Waals forces, other procedures can be carried out to strengthen the final porous material. The PVA molecules present in the surfactant-stabilized system for example were observed to strengthen the structure by concentrating themselves within the contact points between adjacent particles after drying. Cross-linking of such PVA necks with citric acid or sodium tetraborate made these structures stable against dissolution in aqueous media. Alternatively, mechanically stable structures were also obtained by heat treating the material at 800 °C for 2 h, which led to partial sintering and the formation of necks between adjacent silica particles without affecting the interstitial pore sizes.

Since the formation of porous structures using this approach does not rely on specific chemical reactions, the method is very general and applicable to droplets, colloidal particles, and surfactant systems of various chemical compositions. To illustrate this versatility, we also produced hierarchical porous structures from complex suspensions containing octane droplets, polystyrene particles, CTAB, and hydrolyzed TEOS. The hydrolyzed TEOS acts as the precursor for the silica that forms the final structures. The structure obtained after drying exhibits 140 μm monodisperse open pores (Figure 4d) surrounded by 400 nm polystyrene particles containing precipitated silica within their interstices (Figure 4e). The polystyrene particles of the as-dried material were removed by thermal decomposition at 500 °C for 2 h to form 400 nm open pores with silica walls surrounding the larger 140 μm pores. The thickness of the silica wall was tuned by varying the initial concentration of hydrolyzed TEOS in the initial complex suspension (Figure 4f).

Another possible approach is to infiltrate *a posteriori* the interstices between colloidal particles with well-established metal alkoxide/surfactant solutions to generate mesoporous walls of tailored compositions after thermal treatment, thus incorporating an additional length scale in the structure. Since the presence of TEOS concentrations higher than 1 mol/L in the initial continuous phase tend to cause agglomeration between the colloidal particles, the infiltration of structures after drying is a more flexible approach to obtain larger infiltrated areas and to control the chemical composition, porosity, and thickness of the pore walls.

Close observation of the dried structures reveals that ordered arrays of colloidal particles are formed in the vicinity of the droplet-templated windows, whereas less ordered particle ensembles are observed away from this region (Figure 4e). The formation of ordered structures close to the windows is caused by the drying-induced capillary flow of colloidal particles into the thin

aqueous film formed next to the particle-free region where the droplets are closest to the air−liquid interface (Figure 2d).[48,49] Such flow of colloidal particles toward the edge of the evaporating drop was indeed observed during drying of our complex suspensions (see video S2 in the Supporting Inormation).

To further demonstrate the potential of our approach, the capillary flow of particles was combined with the buoyant effect of light droplets to form truly 3D hierarchical porous structures, as illustrated in Figure 5. Structures exhibiting pores at three length scales ranging from tens of nanometers to a couple of millimeters in size were achieved by filling the holes of a 3D glass substrate with a complex suspension of droplets, particles, and surface active molecules. In this case, buoyancy forces pull the octane droplets to the top of the suspension in all the holes (Figure 5a). Pinning of the suspension surface at the upper edge of the substrate during the drying process allows for the deposition of creamed droplets on the vertical walls of the holes and leads to the formation of a thinning film that induces capillary flow of colloidal particles toward the upper surface of the complex suspension (Figure 5a1,a2). The pores of the 3D hierarchical structure obtained using this approach are defined by the holes of the substrate, the droplets, and the interstices between the colloidal particles. An additional hierarchical level containing mesopores can be achieved in this system by simply using the polystyrene particles depicted in Figure 4e and infiltrating the particle interstices with well-established metal alkoxide/surfactant solutions before ultimately removing the polymeric particles. As long as pinning and full wetting of the complex suspension on the 3D substrate is ensured, the method can potentially be extended to many other systems with different chemical compositions and combinations of substrates, templating droplets, colloidal particles, and molecular species.

4. Conclusions

We show that monodisperse and ordered hierarchical materials with precisely controlled porous structure can be obtained through the self-assembly of droplets, colloidal particles, and molecular species induced by simple drying of a complex suspension. Interconnected macropores are achieved in the case where the droplets are stabilized by long-chain surfactants, whereas close macroporosity is obtained when droplets are stabilized by interfacially adsorbed colloidal particles. The dynamics of the drying process can be quantitatively described using simple interfacial tension arguments combined with a phenomenological model that predicts the flux of fluids through a porous particle packing. The unique 3D hierarchical porous structures formed using this simple route can potentially lead to enhanced performance and offer novel functionalities in filtration, catalysis, sensing, and regenerative medicine.

Acknowledgment. We thank Dr. Thomas R. Dietrich (Mikroglas Chemtech GmbH, Mainz, Germany) for kindly supplying the structured glass substrates. A.R.S. thanks the Swiss National Science Foundation for the financial support (Grant PBSK2-116386/1). The work at Harvard University was supported by the NSF (DMR-0602684) and the Harvard MRSEC (DMR-0820484).

Supporting Information Available: The supporting information contains a video showing the self-assembly of droplets at the air−water interface, videos of the drying process of surfactant- and particle-stabilized droplets, a complete analysis of the dynamics of the droplet evacuation process, and a comparison between the size distribution of droplets and final macropores. This material is available free of charge via the Internet at http://pubs.acs.org.